Références

BRADLEY, C. C., GEBBIE, H. A., GILBY, A. C., KECHIN, V. V. & KING, J. H. (1966). *Nature, Lond.* **211**, 840.

BRIDGMAN, P. W. (1942). *Proc. Amer. Acad. Arts and Sci.* **74**, 399.

BUSING, W. R., MARTIN, K. O. & LEVY, H. A. (1962). *ORFLS*. ORNL-TM-305, Oak Ridge National Laboratory, Oak Ridge, Tennessee.

BUSING, W. R., MARTIN, K. O. & LEVY, H. A. (1964). *ORFFE*. ORNL-TM-306, Oak Ridge National Laboratory, Oak Ridge, Tennessee.

CLAVAGUERA-PLAJA, N. (1970). Thèse Doct. Troisième Cycle, Orsay.

DOEDENS, R. J. (1970). In *Crystallographic Computing*, p. 198. Copenhagen: Munksgaard.

DRICKAMER, H. G. (1967). *Science*, **156**, 1183.

FOURME, R. (1968). *J. Appl. Cryst.* **1**, 23.

FOURME, R. (1969). *C. R. Acad. Sci. Paris*, **268C**, 931.

FOURME, R. (1970). Thèse Doct., Paris.

HENSHAW, D. E. (1961). *Acta Cryst.* **14**, 1080.

HYBL, A., RUNDLE, R. E. & WILLIAMS, D. E. (1965). *J. Amer. Chem. Soc.* **87**, 2779.

JOHNSON, C. K. (1965). *ORTEP*. Report ORNL-3794. Oak Ridge National Laboratory, Oak Ridge, Tennessee.

LA PLACA, S. J. & IBERS, J. A. (1965). *Acta Cryst.* **18**, 511.

LIPPINCOTT, E. R., WEIR, C. E., VAN VALKENBURG, A. & BUNTING, E. N. (1960). *Spectr. Acta*, **16**, 58.

PAWLEY, G. S. (1969). *Acta Cryst.* A**25**, 531.

PIERMARINI, G. J., MIGHELL, A. D., WEIR, C. E. & BLOCK, S. (1969). *Science*, **165**, 1255.

RENAUD, M. & FOURME, R. (1967). *Acta Cryst.* **22**, 695.

SCHERINGER, C. (1963). *Acta Cryst.* **16**, 546.

SCHOMAKER, V. & TRUEBLOOD, K. N. (1968). *Acta Cryst.* B**24**, 63.

VALKENBURG, A. VAN (1962). In *High Pressure Measurements*, p. 87. Washington: Butterworths.

VALLINO, M. (1969). *J. Organometal. Chem.* **20**, 1.

VU, H. (1970). Communication privée.

WEIR, C. E., BLOCK, S. & PIERMARINI, G. J. (1965). *J. Res. Natl. Bur. Stands.* **69C**, 275.

WEIR, C. E., PIERMARINI, G. J. & BLOCK, S. (1969). *Trans. A.C.A.* **5**, 105.

Acta Cryst. (1971). B**27**, 2380

Reflection Intensity Measurement by Screenless Precession Photography

BY NGUYEN-HUU XUONG AND STEPHAN T. FREER

Departments of Chemistry, Biology and Physics, University of California, San Diego, La Jolla, California 92037, *U.S.A.*

(*Received* 11 *January* 1971)

When the layer-line screen is discarded the crystal irradiation time required to expose a set of intensity data films with the precession camera can be reduced by an order of magnitude. Although the resulting diffraction pattern is too complex to be indexed by inspection, it can be readily interpreted by computer. The theory and practice of screenless precession photography are presented: mathematical expressions giving the film coordinates of recorded reflections are derived, the technique of film measurement with an automatic scanning densitometer is explained, the film-processing computer programs are described, the strategy for data collection is outlined, and intensity data measured by the screenless precession method are compared with data measured by an automatic diffractometer.

Introduction

The precession camera is used in many laboratories for measurement of X-ray intensity data. Usually, a layer-line screen is mounted on the camera to block out all reflections except those lying in a single plane of the reciprocal lattice; the films can then be indexed by inspection and measured with a simple microdensitometer. But, as we pointed out in an earlier communication (Xuong, Kraut, Seely, Freer & Wright, 1968), the advent of the automatic densitometer directly linked either to a small computer or to a magnetic tape drive (Abrahamsson, 1966; Arndt, Crowther, & Mallett, 1968; Xuong, 1969) makes it possible to dispense with the layer-line screen because the resulting diffraction pattern, although complex, can be readily indexed by computer. Such screenless precession photography offers advantages over normal layer-line screen precession photography, particularly for crystals with large unit cells: the efficiency of data collection is greatly increased since all diffracted rays are recorded on the film; exposure time is cut down by an order of magnitude because a smaller precession angle, *e.g.*, 2° instead of 21°, is required; and precise alignment of the crystal is not necessary in the absence of a layer-line screen (Xuong *et al.*, 1968).

We here present the theory and practice of screenless precession photography. We first derive expressions giving the film coordinates of recorded reflections, explain the technique of film measurement, and then describe the film-processing computer programs. Finally, we outline the strategy for data collection and discuss the quality of the intensity data obtained with this method.

Calculation of the film coordinates for recorded reflections

In this section are derived expressions that relate the position at which a reflection is recorded on the film to the precession angle μ, the wavelength of the incident irradiation λ, the crystal unit-cell parameters, and the orientation of the crystal. Frequent reference is made to Fig. 1, a representation of the precession diffraction geometry. The notation is similar to that of Buerger (1964) and is explained in the text.

The film position of each reflection is specified by coordinates (X,Y) in a Cartesian coordinate system with its origin at O', the point on the film which remains invariant during precession (the incident beam strikes the film at O' when there is no film advance), and with the X axis parallel to the camera spindle axis (the positive direction is from left to right when viewed from the crystal). The position of a general reciprocal-lattice point, P, is described in three-coordinate systems.

(1) The crystallographic reciprocal-lattice system

$$\vec{OP}=ha^*+kb^*+lc^* .$$

(2) A Cartesian coordinate system with its origin at O, the origin of the reciprocal lattice, and with the x axis parallel to the film X axis, the y axis parallel to the film Y axis, and the z axis perpendicular to the plane of the film and directed toward the X-ray sources:

$$\begin{aligned} x&=ha_x^*+kb_x^*+lc_x^* \\ y&=ha_y^*+kb_y^*+lc_y^* \\ z&=ha_z^*+kb_z^*+lc_z^* . \end{aligned}$$

where a_x^* is the projection of the a^* axis onto the x Cartesian axis, *etc.*

(3) A cylindrical coordinate system, (ξ,φ,ζ), again centered at O, and with the cylindrical ζ axis identical to the z axis of the Cartesian system

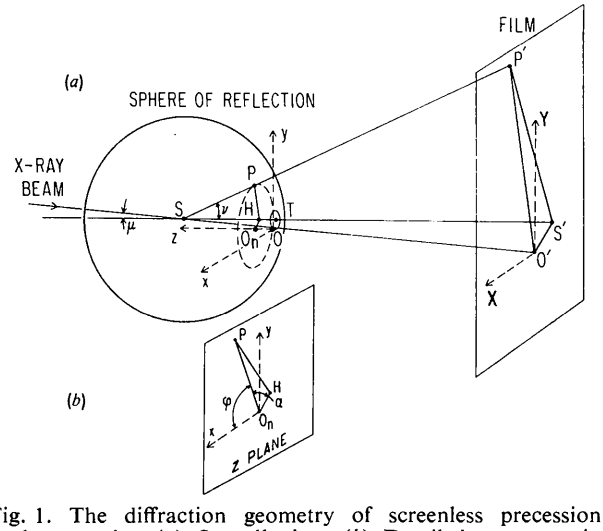

Fig. 1. The diffraction geometry of screenless precession photography. (*a*) Overall view. (*b*) Detailed geometry in the rational plane of the diffracting reciprocal-lattice point P.

$$\begin{aligned} \xi&=(x^2+y^2)^{1/2} \\ \varphi&=\tan^{-1} y/x \\ \zeta&=z . \end{aligned}$$

The point P' at which the scattered beam strikes the film is specified by vector $\vec{O'P'}=\vec{O'S'}+\vec{S'P'}$ where S' is the foot of the perpendicular to the plane of the film from the center, S, of the sphere of reflection; the angle between this perpendicular and the incident beam is $\bar{\mu}$, the precession angle. Thus the film coordinates of a recorded reflection are:

$$X=(\vec{O'S'})_X+(\vec{S'P'})_X \tag{1}$$

$$Y=(\vec{O'S'})_Y+(\vec{S'P'})_Y \tag{2}$$

where $(\vec{O'S'})_X$ is the projection of $\vec{O'S'}$ along the X axis, *etc.* Now, $\vec{O'S'}$ and $\vec{S'P'}$ can be expressed in terms of vectors $\vec{O_nH}$ and $\vec{HP}$ which, in turn, are directly related to the position of the reflecting reciprocal-lattice point:

$$\vec{O'S'}=\vec{OT}\cdot\frac{SO'}{SO}=\vec{O_nH}\cdot\frac{SO'}{SO} \tag{3}$$

$$\vec{S'P'}=\vec{HP}\cdot\frac{SS'}{SH} . \tag{4}$$

The points O_n, H, and P lie in the z plane, the rational reciprocal-lattice plane through the reflecting reciprocal lattice point P and parallel to the plane of the film. Points O_n and H are the intersections of Oz and SS' with the z plane and point T is the intersection of SS' with the zero-level plane. Triangle O_nHP is redrawn in Fig. 1(*b*). Substituting for $O'S'$ and $S'P'$ in (1) and (2),

$$X=(\vec{O_nH})_x\frac{SO'}{SO}+(\vec{HP})_x\frac{SS'}{SH} \tag{5}$$

$$Y=(\vec{O_nH})_y\frac{SO'}{SO}+(\vec{HP})_y\frac{SS'}{SH} . \tag{6}$$

Equations (5) and (6) can be put in more fundamental terms. Letting $f=SO'$, the crystal-to-film distance, and noting that the radius of the sphere of reflections is $1/\lambda$, we have $SO'/SO=f\lambda$. From $SS'=SO'\cos\bar{\mu}=f\cos\bar{\mu}$ and $SH=ST-TH=1/\lambda\cos\bar{\mu}-z=(\cos\bar{\mu}-z\lambda)/\lambda$, we get $SS'/SH=\lambda f\cos\bar{\mu}/(\cos\bar{\mu}-z\lambda)$. Since $O_nH=OT=1/\lambda\sin\bar{\mu}$, the x component of $\vec{O_nH}$ becomes $1/\lambda\sin\bar{\mu}\cos\beta$, where $\beta=$angle xO_nH; for $(\vec{HP})_x$ we use $x-(\vec{O_nH})_x$. Expressions for the y components follow and the coordinates of a recorded reflection can now be given by

$$X=f\sin\bar{\mu}\cos\beta+(x-\frac{\sin\bar{\mu}}{\lambda}\cos\beta)\frac{\lambda f\cos\bar{\mu}}{\cos\bar{\mu}-z\lambda} \tag{7}$$

$$Y=f\sin\bar{\mu}\sin\beta+(y-\frac{\sin\bar{\mu}}{\lambda}\sin\beta)\frac{\lambda f\cos\bar{\mu}}{\cos\bar{\mu}-z\lambda}\ . \quad (8)$$

To determine angle $\beta=xO_nH=xO_nP+PO_nH$ we note that angle xO_nP is the polar angle φ which is measured clockwise when viewed with the incident X-ray beam pointing toward the observer [see Fig. 1(*b*)] and that angle α, the magnitude of angle PO_nH, can be derived from the law of cosines

$$\cos\alpha=\frac{O_nP^2+O_nH^2-HP^2}{2\,O_nP\cdot O_nH}=\frac{\xi^2\lambda^2+\sin^2\bar{\mu}-\sin^2\bar{\nu}}{2\,\xi\lambda\sin\bar{\mu}} \quad (9)$$

since $HP=1/\lambda\sin\bar{\nu}$ and $O_nP=\xi$. From $SH=ST-TH$, the relationship between $\bar{\nu}$ and $\bar{\mu}$ follows

$$\cos\bar{\nu}=\cos\bar{\mu}-z\lambda\ . \quad (10)$$

There are two possible values for the angle β,

$$\beta_1=\varphi+\alpha \text{ and } \beta_2=\varphi-\alpha\ , \quad (11)$$

and both values must be used because each reflection is, in general, recorded twice on the film; this double recording causes the splitting of upper level reflections (see Buerger, 1964, p. 92). To minimize the splitting the film may be advanced by δ toward the crystal along the film normal; the film advance is determined empirically and is usually about 0·1 f. Equations (7) and (8) may be rewritten to include δ if we note that SS' becomes $f\cos\bar{\mu}-\delta$ while vector $S'O'$ remains unchanged

$$X_i=f\sin\bar{\mu}\cos\beta_i+(x-\frac{\sin\bar{\mu}\cos\beta_i}{\lambda})\times(f\cos\bar{\mu}-\delta)\frac{\lambda}{\cos\bar{\mu}-z\lambda} \quad (12)$$

$$Y_i=f\sin\bar{\mu}\sin\beta_i+(y-\frac{\sin\bar{\mu}\cos\beta_i}{\lambda})\times(f\cos\bar{\mu}-\delta)\frac{\lambda}{\cos\bar{\mu}-z\lambda} \quad (13)$$

with $i=1, 2$ for the two positions at which the reflection is recorded. Usually the reflection splitting, defined by $\Delta X=X_1-X_2$ and $\Delta Y=Y_1-Y_2$, is small and a reflection is recorded at $X=(X_1+X_2)/2$ and $Y=(Y_1+Y_2)/2$. For completeness, formulae for the Lorentz and polarization factors (Buerger, 1964) in the present notation are

$$\frac{1}{L_i}=\xi\sin\bar{\mu}\sin\alpha\,(1+\tan^2\bar{\mu}\sin^2\beta_i) \quad (14)$$

and

$$P=1-\tfrac{1}{2}[(\xi^2+\zeta^2)\lambda^2]+\tfrac{1}{8}(\xi^2+\zeta^2)^2\lambda^4\ . \quad (15)$$

Equations (9) to (13), together with the appropriate coordinate transformations, are sufficient to determine the film coordinates of a recorded reflection from the reflection indices, unit-cell parameters, and camera parameters. We can thus index a film if we know which reciprocal-lattice points are recorded on it.

The portion of the reciprocal lattice that can be recorded on a single film, for a particular orientation of the crystal, may be determined by examining both the theoretical limits imposed by the diffraction geometry and the experimental restrictions imposed by the size of the film and the size of the diffracted spot on the film. The theoretical restrictions determine which reflections will give rise to scattering, the film-size restrictions determine which of the scattered rays will intercept the film, and the spot-size restrictions determine which of the recorded reflections must be rejected because they are either recorded only partially or overlap each other on the film.

In order for diffraction to occur at all, the following three conditions must be satisfied. (1) A reciprocal-lattice point must intercept the sphere of reflection. (2) Angle $\bar{\nu}$ must be real, *i.e.*, from equation (10):

$$-1\le\cos\bar{\mu}-z\lambda\le 1\ . \quad (16)$$

(3) From triangle O_nPH, the magnitude of the polar radius vector $\xi=O_nP$ must be between the two values $\xi_{max}=HP+O_nH$ and $\xi_{min}=HP-O_nH$ for each reciprocal-lattice level. In other words, for each z plane

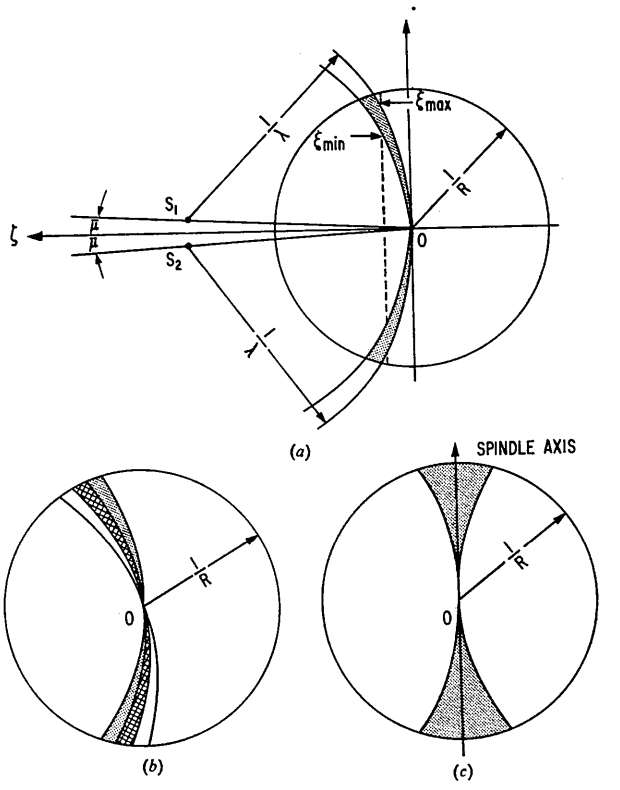

Fig. 2. Sections through the origin of the reciprocal lattice drawn to illustrate the range of recordable reflections. (*a*) The region recorded on one exposure with precession angle $\bar{\mu}$. (*b*) Adjacent regions recorded on three successive exposures with the spindle dial advanced by 2 $\bar{\mu}$ between exposures. (*c*) The region that cannot be recorded without reorienting the crystal with respect to the spindle axis.

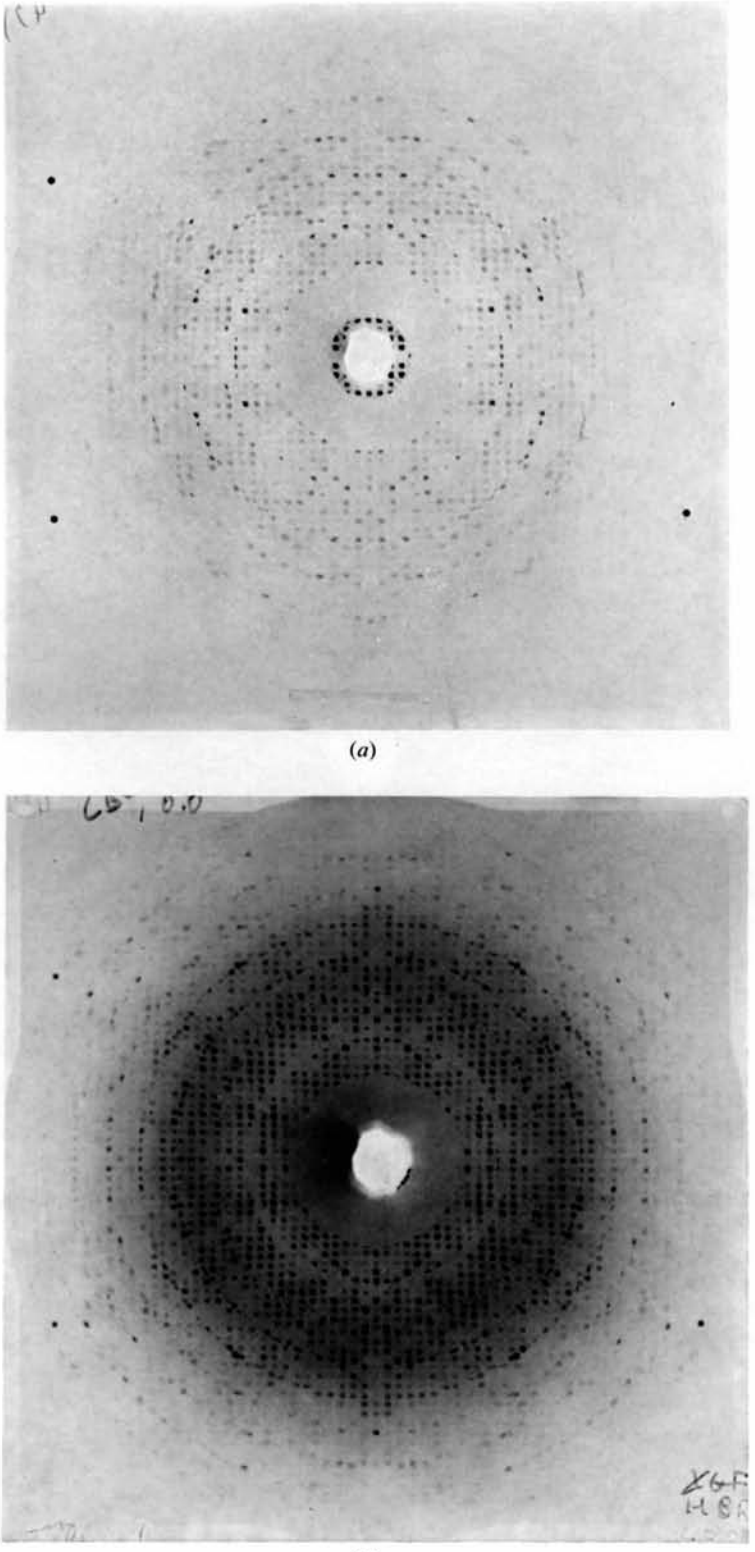

(*a*)

(*b*)

Fig. 3. Typical screenless precession films. (*a*) Line up film. (*b*) Data film with a principal axis along the incident X-ray beam.

[*To face p.* 2382

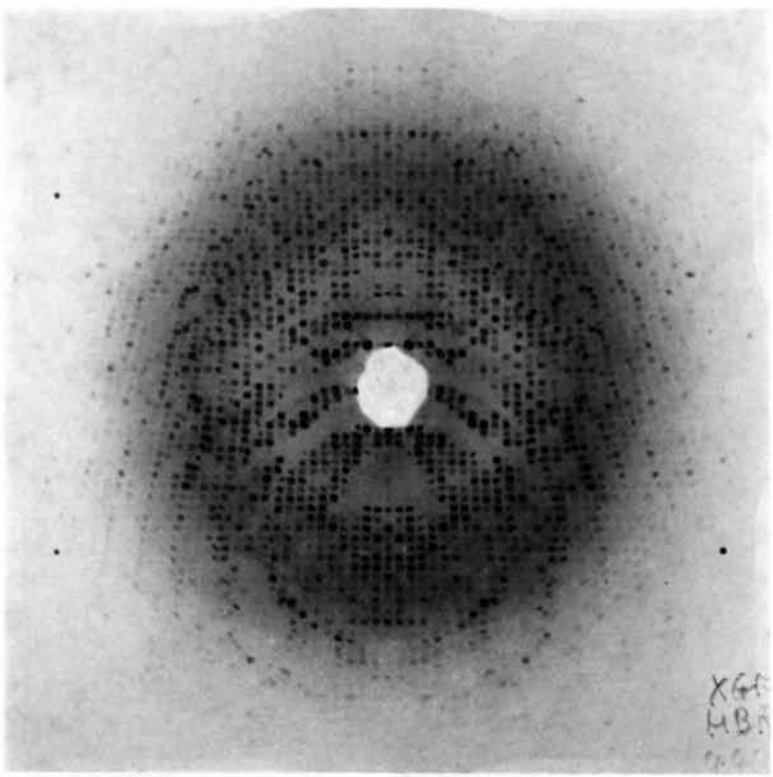

(*c*)

Fig. 3 (*cont.*) (*c*) Data film taken after the spindle dial was rotated by 18° from the orientation for film *b*.

$$\xi_{max} = \frac{1}{\lambda}(\sin \bar{\nu} + \sin \bar{\mu}) \quad (17)$$

and

$$\xi_{min} = \frac{1}{\lambda}(|\sin \bar{\nu} - \sin \bar{\mu}|) . \quad (18)$$

Fig. 2(*a*) is a section through the reciprocal-lattice that shows, within the shaded area, the region satisfying the above conditions. Since the Figure is cylindrically symmetrical about the z axis, the complete region of the reciprocal lattice that can be recorded for a single orientation of the crystal is shaped like a shallow bowl which is thicker at the rim than at the center. The construction of Fig. 2(*a*) can be most easily understood if we consider the crystal and film to be fixed while the X-ray source, and hence the sphere of reflection, precess about the z axis (this is equivalent to the normal precession of the crystal and film about a fixed source, since the relative motions of crystal, film, and source are the same in both cases). In any reciprocal-lattice plane containing the z axis, the maximum excursions of the center of the sphere of reflection during one complete precession cycle are S_1 and S_2. Thus, the potentially recordable portion of the reciprocal lattice lies in the region between the two spheres of reflection centered at S_1 and S_2. The only further restriction is the limit of resolution, R, shown in section by the circle of radius $1/R$ drawn about the origin of the reciprocal lattice.

Experimental parameters determine which of the diffracting reciprocal-lattice points give rise to usable reflection intensities. If the diffracted ray is to be intercepted by the film, the film coordinates, X and Y, must lie within the area of the film. In addition, a complete reflection cannot be recorded for reciprocal-lattice points that lie too near the cut-off limits ξ_{min} and ξ_{max}. Only a portion of the diffracted ray is produced when ξ is too near either of these limits, that is, if c, as given by

$$c = f\lambda|\xi_{max} - \xi| \quad (19)$$

or

$$c = f\lambda|\xi_{min} - \xi|, \quad (20)$$

is smaller than the film spot size for this reflection. An additional reason for rejecting reflections that are near the cut-off limits is the rapid variation of the Lorentz factor in this area of the film. This is evident from examining equation (14) and noting that the extrema in ξ occur when α is either 0 or 180°. Finally, reflections for which all or a part of the diffracted rays intercept the same area on the film cannot readily be used for measurement of intensity data.

Film measurement

There are two types of films used in data collection by screenless precession photography: (1) line-up pictures for the precise measurement of crystal orientation [see Fig. 3(*a*)] and (2) the actual data films from which integrated intensities are measured [see Fig. 3(*b*) and 3(*c*)]. The exposure time required for line-up pictures is typically one fifth the exposure time required for data films. Near the edges of every picture are three dark reference points obtained by shining light through holes drilled in the back of the film cassette. These fiducial marks are easily recognized on the film because they are always darker than any reflections in the immediate neighborhood. The fiducial marks are used in four ways: (1) to aid in determining the crystal orientation from the line-up picture; (2) to distinguish the front and back surfaces of the film (the three marks form the letter 'L' when the viewer is looking in the direction of the X-ray beam); (3) to allow automatic determination of the film orientation on the scanner by computer program; and (4) to allow determination of film shrinkage in both the X and Y directions.

The three correction angles needed to specify the crystal orientation from the line-up films (Buerger, 1964, p. 114) are determined from (*a*) the position of the zero-level circle relative to the center of the diffraction pattern and (*b*) the angle between the near-horizontal crystal axis and the horizontal reference axis joining the two lower fiducial marks. The details of the correction-determination are presented in Fig. 4 and a typical line-up picture is shown in Fig. 3(*a*). The small-angle approximation used in the derivation of the equations in Fig. 4 (Buerger, 1964, p. 114) limits the magnitude of the correction angles φ_1 and φ_2 to less than one degree for valid orientation determination. The determination of the correction angles allows us to forego the time-consuming and tedious procedure of precise alignment of the crystal on the camera.

Two data films are shown in Fig. 3(*b*) and (*c*). Fig. 3(*b*) is an a^* projection with a relative spindle dial setting of 0° ($\tau = 0°$). In this film it is possible to recognize the individual levels (the zero level is obscured by the beam stop) and hence to index the reflections by inspection; the overlapping of adjacent levels does not occur until the fourth level. The reflections near the inner and outer edge of each level are only partially recorded (see equations 19 and 20) and usually appear relatively dark on the film since the corresponding reciprocal-lattice points pass tangentially through the sphere of reflection. The film in Fig. 3(*c*) was obtained from the same crystal orientation but with spindal dial rotated by 18° ($\tau = 18°$). It is evident that it is impractical to index the reflections on this film without the aid of a computer.

In order to accurately measure the entire range of diffracted intensities, a pack of two films is used for each data-film exposure.

The digital scanning densitometer system employed for processing the data films (Xuong, 1969) consists of a rotating-drum scanning densitometer linked to an IBM 1800 computer equipped with a magnetic disk drive. In five minutes the scanner is able to scan an entire 5×5 in film, sampling it on a 200×200 μm raster, and transfer the entire digitized film image (about

350,000 optical density measurements) to the computer to be stored on the magnetic disk. The optical density measurements range from 0·0 to 2·2, with 256 grey levels and the optical density reading is standardized against the incident light beam on every scanning line, thereby eliminating most of the instabilities inherent in optical density measurement. Because of the rapid access capabilities of the disk memory, integrated intensities can be efficiently evaluated from the digitized film image by computer programs. A series of nine programs handles all the processing automatically; an operator is required only to put the films on the scanner. The performance of the scanning system has been very satisfactory: the center of a spot on the film can be determined with an accuracy better than $\pm 100\ \mu m$; repeated measurements of the integrated intensity of the same reflection placed at different positions on the scanner do not differ by more than $\pm 1\%$; the individual optical density measurement itself has a precision of ± 2 levels over the entire range of 256 grey levels; and, finally, the scanner has been in continuous operation for two years with very little maintenance and without a single major breakdown.

Film processing programs

There are two possible ways to index screenless precession films: one is to determine the index from the position of the reflection on the film, as is commonly done for layer-line screen films, and the other is to calculate the position of the center of the spot from the indices of the reflection, analogous to the practice in diffractometer data collection. The latter method is more practical since it avoids the intricacy of pattern recognition and the mathematics are straightforward. Accordingly, the film-processing programs index reflections by generating all *hkl* within the resolution limit and calculating the film coordinates of only the reflections that are recorded on the film [reflections satisfying the conditions of equations (16) to (20)].

Table 1. *Film processing programs*

	Program	Function
	VTNM	Generates indices for all reflections within a specified resolution limit and determines the film coordinates (X, Y) and Lorentz-polarization factors for the recorded reflections.
	SØRTX	Sorts all reflections on X and Y.
	ELIM	Eliminates all overlapped or near-edge reflections and stores the remaining reflections in file 1 of the disk.
Repeated for each film	SCANR	Accepts the optical density measurements from the automatic densitometer and stores them in file 2 of disk.
	SETA	Measures the positions of the film fiducial marks and determines the center and the orientation of the diffraction pattern.
	SAGON	Estimates integrated intensities.
	SCAL	Scales intensities from films 1 and 2.
	SORTH	Sorts reflections in h, k, ℓ order.
	PNHKL	Outputs h, k, ℓ, F^2 and σ for all observations.

A list of the nine computer programs that are used to process intensity data films is shown in Table 1. The programs are divided logically into three blocks of three programs each, which are concerned with: (*a*) index generation, (*b*) film processing and (*c*) data merging and output of results. The programs are general in that they will process films taken either with or without a layer-line screen.

From the unit-cell parameters, camera parameters, and crystal orientation, the program *VTNM* finds the indices, *hkl*, of all reflections that are recorded on the two films of the data-film pack. It then calculates the film coordinates (X,Y), the Lorentz–polarization factor, and both the magnitude and direction of the spot splitting for each of these reflections. The program *SORTX* now sorts these reflections into increasing order with respect to the film coordinates (X,Y) in order to allow program *ELIM* to eliminate efficiently all overlapping and near-edge reflections. In the present version of the program these reflections are discarded; typically they constitute from 25 to 40% of the total reflections on the film (Xuong *et al.*, 1968). The remaining usable reflections are then stored on file one of the magnetic disk.

After the above three preliminary programs are run, the darker film of the data pack is placed on the scanner and program *SCANR* is initiated. *SCANR* accepts the digitized optical density measurements from the scanner and stores them on file two of the magnetic disk. In order to automatically process this digitized film image, the

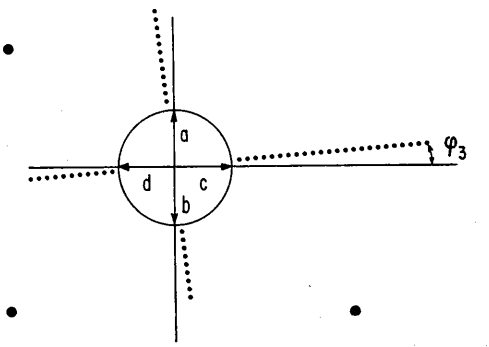

Fig. 4. Schematic representation of the zero-level circle and the axes of the diffraction pattern (dotted lines) of a line-up film. The formulae for the three orientation correction angles are:

$$\varphi_1 = \frac{(a-b)}{4f} \times \frac{180}{\pi}, \quad \varphi_2 = \frac{(c-d)}{4f} \times \frac{180}{\pi}, \quad \varphi_3 = \text{angle between}$$

a crystal axis and the axis defined by the horizontal fiducial marks.

computer must 'know' precisely how the film is positioned on the scanner. Program *SETA* accomplishes this by finding the three fiducial marks on the film (these are darker than any adjacent reflections) and determining their location relative to the scanning axis. This program also determines the X and Y film-shrinkage corrections by comparing the distance between the fiducial marks on the film with the known distance between the holes drilled in the film cassette.

The job of estimating integrated intensities is left to the program *SAGON*. This program first reads file one of the disk to retrieve the index and orientation-dependent information for the next reflection to be processed, in particular its calculated film coordinates. The optical density measurements of a small area of the film around this position are then retrieved from file two of the disk. The observed center of the reflection is taken to be the center of that 3×3 matrix of raster points which yields the highest sum of optical density readings when the center of the matrix is successively moved ± 1 raster point in the X and Y directions from the calculated position (if the maximum sum exceeds a predetermined level, the difference between the calculated and observed coordinates of the reflection is stored and used as an empirical correction to be applied to the calculated coordinates of neighboring reflections). The program then calculates the integrated intensity from the optical density measurements which lie inside an area determined by spot size and splitting (see Fig. 5) and estimates the background from the optical density measurements of the raster points immediately adjacent to this area (the background points always exist since *ELIM* rejects spots that are not separated by at least one raster point). The integrated intensity (minus background) is multiplied by the Lorentz–polarization factor and, together with the estimated sampling error and the reflection indices, stored in file three of the disk.

The three programs, *SCANR*, *SETA* and *SAGON* must be repeated for the second film of the data film pack. However only 10 or 20% of the reflections on the second film are processed: reflections that are either too dark to be measured on film one or are needed for scaling the two films of the data pack together.

Program *SCAL* scales the reflection intensities from films one and two and program *SORTH* sorts them into the desired index order. The intensity data are then output on either binary cards or magnetic tape.

The above programs are now running on-line on an IBM 1800 computer using one magnetic disk. However, it is also possible to write the digitized film image directly onto a magnetic tape and have it processed on an off-line computer. Accordingly, some of the above programs have been rewritten for an IBM 360 computer by Dr G. Cohen of U.S. National Institutes of Health.

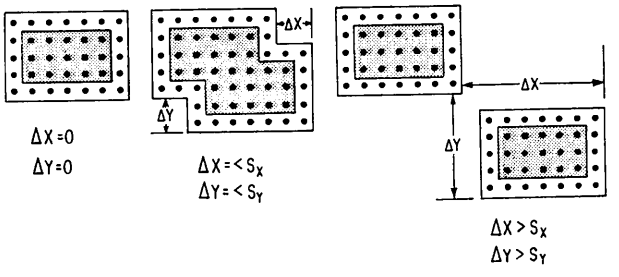

Fig. 5. Integrated intensity measurements of reflections with different degrees of splitting. The dots represent the optical density sampling raster, the peak intensity is integrated within the entire shaded area, and the background is estimated from the immediately surrounding raster points. $S_x(S_y)$ and $\Delta X(\Delta Y)$ are the spot dimensions and splitting of the reflections in the film $X(Y)$ direction. For $\bar{\mu}=2{\cdot}5°$, and $f=75$ mm, ΔX and ΔY vary from 0 to about 1·5 mm.

Data collection procedure

With screenless precession photography the general procedure for measuring a high precentage of unique reflections out to the desired resolution is to mount the crystal in a favorable orientation and then expose a series of films with the spindle dial setting advanced by a predetermined fixed increment between each exposure. In order to minimize crystal irradiation it is first necessary to determine the optimum crystal orientation and optimum values for the camera parameters f and $\bar{\mu}$.

To assure minimum overlapping of reflection from adjacent levels the crystal should be oriented so that the longest real axis lies along the spindle axis.

The crystal-to-film distance, f, is determined once the desired resolution is selected. The resolution of the data is independent of $\bar{\mu}$ and depends only on the diffracting power of the crystal, the dimensions of the film, and the crystal-to-film distance (this is contrary to normal layer-line screen precession photography in which the resolution depends on $\bar{\mu}$). For proteins, the diffracting power of the crystal usually limits the resolution to 2 to 2·5 Å. The resolution limit and the size of the film determine the maximum f; this value should be used in order to minimize the overlapping of reflections from different levels.

To choose the optimum precession angle for a particular crystal orientation and a particular f, the first three computer programs shown in Table 1 are run with different values of $\bar{\mu}$, *e.g.*, with $\bar{\mu}$ varying from 1 to 3° in 0·25° increments, in order to select the value that gives the greatest efficiency ratio. The efficiency ratio is the number of usable reflections on a film divided by the total number of reflections recorded on that film (Xuong, *et al.*, 1968).

To determine the film-to-film dial setting increment, $\Delta\tau$, it is nessary to examine the region of the reciprocal lattice that is recorded on each film. A section of this region is shown as the shaded area in Fig. 2(*a*). From this Figure it is evident that an immediately adjacent region of the reciprocal lattice will be swept out if the spindle dial setting is incremented by $2\bar{\mu}$; sections of three such adjacent regions are shown in Fig. 2(*b*). Because reflections near the edge of each level are only

partially recorded, they cannot be used and the practical film-to-film dial increment should be reduced by a fraction of a degree, *e.g.*, $\Delta\tau = 2\bar{\mu} - 0{\cdot}5°$. With a particular crystal mounting the total excursion of the spindle dial, or, in other words, the number of films required to measure the unique portion of the reciprocal lattice, obviously depends on the crystal symmetry. There is, however, a small region of the reciprocal lattice that will be missed if only one such series of films is exposed [see Fig. 2(*c*)]. Thus, to measure all the reflections in one asymmetric unit of reciprocal space a second series of films is required. For this series the 'next best' crystal orientation should be used. The two series of films will contain sufficient replicate data for good film-to-film scaling.

Quality of the data

During the last two years we have measured with screenless precession photography a total of 750,000 reflection intensities from four different proteins. The current versions of the film-data processing programs are fairly primitive since they were written for an IBM 1130 computer that has 8K of core memory and a single disk drive with one million bytes of storage. With more core and disk storage the sophistication of the programs can be considerably increased to achieve greater precision and a higher data processing rate.

With the present system the rate limiting step in the measurement of intensity data is the computer-processing of the digitized film image. This now takes about two hours per film and at this rate the system can handle the output of two precession cameras running full time. Since the disk is now referenced once for every reflection, most of the computer time is spent accessing the disk storage. However, more core memory will allow many reflections to be referenced at one time and will thereby considerably increase the processing rate.

For three proteins, chymotrypsinogen A, cytochrome c_2, and subtilisin, intensity data have been measured both with screenless precession films and with a Hilger–Watts four-circle automatic diffractometer. The reproducibility of the film and diffractometer data can be compared by examining the reliability factor

$$R = \frac{\sum |k_i I_i - \langle I \rangle|}{\sum k_i I_i}$$

where k_i is the scaling constant for a particular film or diffractometer data-collection shift, the summation is over all observations, and $\langle I \rangle = 1/N \sum k_i I_i$ is the average intensity for N observations of the same reflection. The reproducibility among the film data, among the diffractometer data, and between the film and diffractometer data is quite good as can be seen in Table 2. In general, the diffractometer data are more reproducible than the film data. However, the chymotrypsinogen data are of equal quality and this probably is due to the relatively longer exposure time used for chymotrypsinogen films. The reliability factors for both film and diffractometer data are very dependent on reflection intensity, but the reproducibility of reflections with approximately equal intensity is indepen-

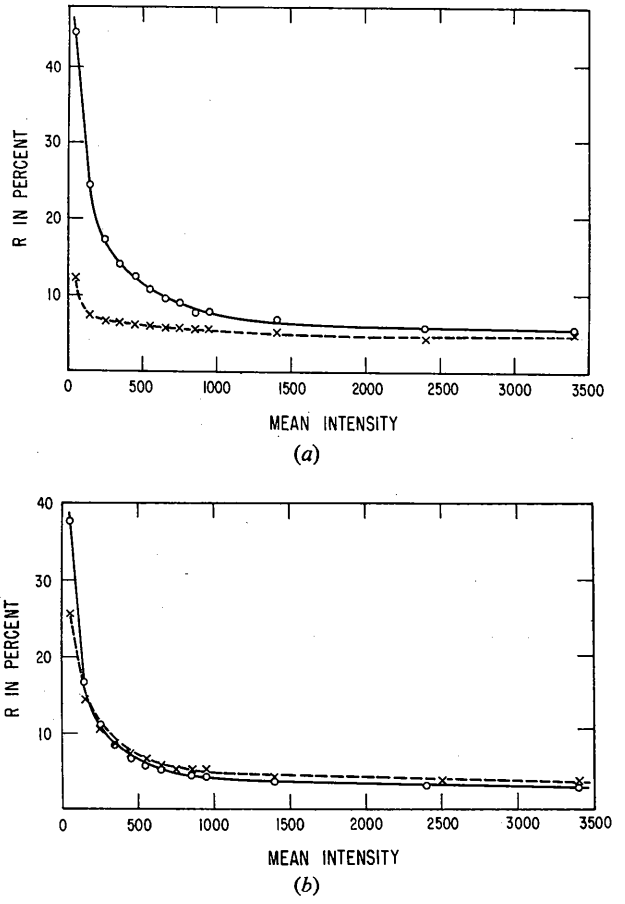

Fig. 6. Variation of the reliability factor with mean reflection intensity for film (open circles) and diffractometer (crosses) data; (*a*) subtilisin and (*b*) chymotrypsinogen.

Table 2. *Reproducibility of film and diffractometer intensity data from three proteins*

	Film		Diffractometer		Combined	
	Number of observations	R	Number of observations	R	Number of obseravtions	R
Chymotrypsinogen	14227	6·34 %	27989	5·86 %	45197	6·78 %
Cytochrome c_2	27379	7·36	12922	3·88	42024	7·30
Subtilisin	89303	9·99	85934	4·89	175663	8·32

$R = \sum |k_i I_i - \langle I \rangle| / \sum k_i I_i$ as defined in the text.
These statistics are from *all* replicated reflections for the parent proteins.

dent of $\sin\theta/\lambda$. Fig. 6 shows the variation of R with intensity for subtilisin and chymotrypsinogen film and diffractometer data. The shapes of the curves are typical of all data we have measured: at high intensity, the curves approach asymptotic minimum R values, but for weak reflections, the film R increases much more rapidly with decreasing intensity than the diffractometer R. This is not surprising because the error in the film data has a minimum floor owing to the constant sampling error (± 2 grey levels for each raster point measurement) whereas the error of the diffractometer data is proportional to $\sqrt{I}$.

It is worthwhile to compare the quality of intensity data obtained from conventional (with layer-line screen) and screenless precession films. A meaningful comparison can only be made by using both methods to measure a significant number of reflections from the same protein. Unfortunately, such data are not now available. We can, however, compare the reproducibility of our data with the reproducibility obtained by the Stockholm group for horse liver alcohol dehydrogenase data (Werner, 1970). These data were collected on conventional precession films and measured with an automatic film scanner. Werner quotes an R_F of 2% for intense $00l$ reflections and an average R_F of 2·7% for 623 overlapping reflections out to 6·0 Å resolution. The range of R_F values for the most intense $\frac{1}{3}$ of our data is from 2·3% for chymotrypsinogen (5041 observations) to 2·7% for subtilisin (13528 observations); the R_F range for our 6·0 Å data is from 4·3% for chymotrypsinogen (714 observations) to 5·4% for subtilisin (4437 observations). It should be emphasized that the screenless intensity data used for this comparison, and also for Table 2 and Fig. 6, were obtained from routine data films and that all applicable multiply-observed reflections were included. Based on the above unsophisticated comparison, we feel that the quality of data collected with screenless precession photography is nearly as good as that collected with conventional precession photography. On the other hand, crystal irradiation time is reduced by an order of magnitude with the new method. Furthermore, improvements in data measurement and processing (see below) will make the quality of screenless precession data even better than it now is.

The practical test of any data collection method is whether the clarity of the electron-density map it yields is sufficient for the purpose of a particular investigation. In this context it was possible, without undue difficulty, to construct a Kendrew–Watson skeletal model of the *chromatium* iron protein HiPIP from an electron-density map obtained with data collected exclusively on screenless precession films (Carter, 1970, private communication). In addition most of the intensity data for the 2·5 Å structure of chymotrypsinogen A (Freer, Kraut, Robertus, Wright & Xuong, 1970) were measured with screenless precession photography. The data for cytochrome c_2 were used to screen heavy-atom derivatives and the subtilisin data are being used to extend the resolution of the present electron-density map to 2·0 Å.

As we indicated above, increased computer capabilities make possible many improvements in the film processing programs. Among the more obvious of these: (1) reduction of the film sampling raster from the present 200×200 μm to 100×100 μm will quadruple the number of measurements per spot and thus greatly increase the precision of the integrated intensities (unfortunately this also quadruples the amount of disk storage required); (2) least-squares refinement of the crystal orientation angles for each film will help compensate for small crystal slippage that may occur when the spindle dial is advanced between exposures; and (3) better detection of the center, size, and shape of each spot will further increase the precision of the intensity measurements.

We wish to thank Professor J. Kraut for his encouragement and Professor W. Vernon and Mr J. Cornelius for their help in setting up the system. Mrs S. Glasser has greatly helped with the programming. This work was initiated with funds from the NIH Biomedical Science Support Grant and is now continued with support from the National Science Foundation and the National Institutes of Health.

References

ABRAHAMSSON, S. (1966). *J. Sci. Instrum.* **43**, 931.
ARNDT, U. W., CROWTHER, R. A. & MALLETT, J. F. W. (1968). *J. Sci. Instrum.* **1**, 510.
BUERGER, M. J. (1964). *The Precession Method.* New York: John Wiley.
FREER, S. T., KRAUT, J., ROBERTUS, J. D., WRIGHT, H. T. & XUONG, NG. H. (1970). *Biochemistry,* **9**, 1997.
WERNER, P. E. (1970). *Acta Cryst.* A**26**, 489.
XUONG, NG. H. (1969). *J. Sci. Instrum.* **2**, 485.
XUONG, NG. H., KRAUT, J., SEELY, O., FREER, S. T. & WRIGHT, C. S. (1968). *Acta Cryst.* B**24**, 289.